Strength improvement in high pressure die-cast Al-Si-Cu alloys by synergistic strengthening of Q-$Al_5Cu_2Mg_8Si_6$ and θ-Al_2Cu phases

Xiangzhen Zhu[a], Xixi Dong[a], Paul Blake[b], Shouxun Ji[a*]

[a] Brunel Centre for Advanced Solidification Technology (BCAST), Brunel University London, Uxbridge, Middlesex UB8 3PH, United Kingdom

[b] Engineering Centre, Jaguar Land Rover, Abbey Road, Coventry, CV34 4LF, United Kingdom

* Corresponding author: Tel.: +44 1895 266663, Fax: +44 1895 269758, Email: shouxun.ji@brunel.ac.uk

Abstract

Die-cast alloys with high strength and acceptable elongation under as-cast condition have been designed and developed by optimising the synergistic strengthening of Q-$Al_5Cu_2Mg_8Si_6$ and θ-Al_2Cu phases in Al-Si-Cu-Mg alloys. It is found that the content of Q-$Al_5Cu_2Mg_8Si_6$ phase could be controlled only by Mg levels, but that of θ-Al_2Cu phase could be affected by Cu and Mg levels. Experimental results demonstrated that the combination of different amount θ-Al_2Cu and Q-$Al_5Cu_2Mg_8Si_6$ phases could provide a same level of yield strength but different levels of elongation. The reasons can be attributed to the differences in morphologies and distributions of θ-Al_2Cu and Q-$Al_5Cu_2Mg_8Si_6$ phases. Microstructural observation confirmed that numerous nanoscale Q-$Al_5Cu_2Mg_8Si_6$ precipitates (mostly under 200nm) were observed inside the α-Al matrix in the developed die-cast alloy. It is anticipated that the Q-$Al_5Cu_2Mg_8Si_6$ precipitates inside the α-Al phase were formed via solid reactions during solidification process. Meanwhile, large Q-$Al_5Cu_2Mg_8Si_6$ phase was also observed as aggregates at the grain boundaries of α-Al phase. θ-Al_2Cu intermetallic were located at the grain boundaries of α-Al phase with blocky or lamellar morphologies. It is also found that exceeding Mg or Cu levels would induce too much strengthening, resulting in the significant decrease in elongation. The optimised strength-ductility trade-off could be achieved with 3.0 wt.% Cu and 0.9 wt.% Mg in a Al-Si alloy, offering the yield strength more than 225 MPa, the ultimate tensile strength more than 360 MPa and the elongation more than 4% under as-cast condition.

Key words:

Aluminium alloys; Microstructure; Mechanical properties; Strengthening mechanism; Precipitate strengthening; Synergistic effect

1. Introduction

High-pressure die casting (HPDC) is a popular process for producing structural components in automotive industry due to its huge advantages in high productivity, good dimensional accuracy and capacity of making complex and thin-wall castings [1, 2]. With the significant progress of HPDC technology derived by increased requirements in the past decades, a series of excellent die-cast Al alloys have been successfully developed for achieving the weight reduction of components [3-6], in which the increased yield strength is essential. At present, the common and effective approach to increase the strength of an alloy is heat treatment to generate precipitates in primary α-Al phase. However, heat treatment consumes energy, causes distortion of thin-wall castings and increases the manufacturing cost, which are unfavourite in industry, in particular the increasing pressure is now facing for reducing the carbon footprint in automotive manufacturing. Therefore, industry really needs a die-cast aluminium alloy capable of offering high strength and elongation with excellent castability under as-cast condition.

After the query of two popular online material property database MatWeb [7] and Matmatch [8], Table 1 lists the available commercial aluminium die-cast alloys with the yield strength (YS) more than 150 MPa under as-cast condition. It is seen that the yield strength of hypoeutectic Al-Si die-cast alloy is generally less than 170 MPa. Although hypereutectic Al-Si die-cast alloys including 390.0, 392.0 and B390.0 can provide the yield strength of more than 200 MPa, the elongation is less than 1%, making these alloys unsuitable for many structural components for dynamic loadings. Al-Mg die-cast alloys show excellent ductility but their yield strengths are still less than 200 MPa [9]. Moreover, the castability, die life and thermal stability of Al-Mg alloys are concerns for wide applications in industry.

The strengthening of metallic materials generally includes (1) grain refinement strengthening, (2) secondary phase strengthening, (3) solid solution strengthening, (4) precipitate strengthening, and (5) work hardening. Among these, work hardening is more effective in wrought alloys, and is significant affected by the defects in cast alloys. Also, the precipitates strengthening works only after solution and ageing heat treatment and is hardly effective for the alloy under as-cast condition. Meanwhile, the grains in HPDC castings is already very fine (less than 20μm) [10-12], further grain refinement is hardly achieved. Therefore, the practical approach for strengthening the die-cast aluminium alloys under as-cast condition is solid solution and secondary phase strengthening, which can be achieved by adding appropriate

alloying elements to enrich α-Al solid solutions with higher solute contents and/or to form secondary phases at grain boundaries. Unfortunately, the strength improvement of cast materials is usually at the expense of ductility. Therefore, the challenge is to find an effective approach to increase the strength with the minimum scarification of elongation. Meanwhile, the important requirement for a cast alloy is that it can make sound castings without increasing the defects levels.

Table 1. Commercial die-cast aluminium alloys (YS>150 MPa) currently available in industry.

Alloy	Main alloying elements	UTS/MPa	YS/MPa	Elongation/%	Equivalent alloys			
					EU	Japan	China	UK
360	AlSi9.5Mg0.5	300	170	2.50	--	--	--	--
A360	AlSi9.5Mg0.5	317	165	3.50	ENAC 43400	ADC3	YL104	LM9
380	AlSi8.5Cu3.5	317	159	2.5	--	--	--	--
A380	AlSi8.5Cu3.5	324	159	3.5	ENAC 46000	ADC10	YL112	LM24
383	AlSi11Cu3	310	152	3.5	--	--	--	--
A383	AlSi11Cu3	310	152	3.5	ENAC 46100	ADC12	YL113	LM2
384	AlSi11Cu3.8	331	165	2.5	--	--	--	--
A384	AlSi11Cu3.8	330	165	2.5	--	--	--	--
390.0	AlSi17Cu4.5Mg0.5	280	240	1.0	--	ADC14	YL117	LM30
B390.0	AlSi17Cu4.5Mg0.5	317	248	1.0	--	--	--	--
392.0	AlSi19Mg1.0Cu0.6	290	270	0.86	--	--	--	--
518.0	AlMg9	310	193	5.0	ENAC 51200	ADC5	--	--

In the present work, we aim to develop a new approach to enhance die-cast aluminium alloys with much improved yield strength and acceptable elongation under as-cast condition, in particular, the yield strength is more than 200MPa and the elongation is more than 4% from standard tensile samples. Based on the analysis of strengthening phases, an innovative approach was used to optimize the synergistic effect of strengthening phases. Experiments were conducted to validate the theoretical understanding. The relationship between solidification, microstructural evolution and mechanical properties were also discussed.

2. Formation of strengthening phases in Al-Si alloys with different Cu and Mg levels

Up to now, many approaches such as adding ceramic particles [13-15] and/or using special melt treatment [16-18] have been developed to strengthen aluminium alloys under as-cast condition. In considering the industrial application, the most common and practically achievable method is alloying because this can maintain the advantages of casting in terms of castability and easy operation. It is generally believed that Al-Si alloys have been widely used because of the good castability and properties. The addition of other elements such as Mg and Cu can strengthen Al-Si alloys [9]. The reported Mg-rich or Cu-rich strengthening phases in Al-Si alloys include β-Mg_2Si, θ-Al_2Cu and Q-$Al_5Cu_2Mg_8Si_6$ and their variations such as θ' and Q' [19-21]. As these are the phases existed in the Al-Si alloys, the question is whether there is a potential for further development of Al-Si alloys using the synergistic strengthening of these elements and phases.

However, it is noticed that abundant β-Mg_2Si, θ-Al_2Cu and Q-$Al_5Cu_2Mg_8Si_6$ cannot be simultaneously formed in one Al-Si alloy. The formation of β-Mg_2Si, θ-Al_2Cu and Q-$Al_5Cu_2Mg_8Si_6$ depends on the Cu and Mg levels, as well as the ratio of Cu to Mg. To understand the relationship between phase formation and Cu/Mg levels, the isothermal section of the Al-8.2Si-0.8Fe-0.5Mn-Cu-Mg alloy (in wt.%, unless otherwise stated) was calculated and shown in Figure 1a. It indicates that the weight percent of Cu/Mg ratio decides the types of phases formed in alloys. When Cu/Mg ratio is less than 0.65, both Q-$Al_5Cu_2Mg_8Si_6$ and β-Mg_2Si phases can be formed. When the Cu/Mg ratio is more than 0.65, both Q-$Al_5Cu_2Mg_8Si_6$ and θ-Al_2Cu phases are formed. Q-$Al_5Cu_2Mg_8Si_6$ phase is the only phase when the Cu/Mg ratio equals to 0.65. Therefore, in practice, only the synergistic strengthening of 2 phases (β+Q, or θ+Q) can be obtained.

By looking the details, the strengthening effect and thermal stability of these intermetallic are different. β-Mg_2Si phase has a good strengthening effect at ambient temperature, but its optimum strengthening effect is obtained only under T6 heat treated condition when β-Mg_2Si exists as nanoscale precipitates in Al matrix. On the other hand, β-Mg_2Si precipitates are easily coarsened at elevated temperatures [22, 23], which limits the application of aluminium alloys in specific areas. Compared with β-Mg_2Si phase, θ-Al_2Cu and Q-$Al_5Cu_2Mg_8Si_6$ phases are more thermodynamically stable. Especially, Q-$Al_5Cu_2Mg_8Si_6$ is relatively fine and stable over 300°C, and several alloys have been reported to use Q-$Al_5Cu_2Mg_8Si_6$ phase to achieve

excellent mechanical properties [20, 24]. Based on the analysis, the favourite strengthening phases in die-cast Al-Si alloys are Q-$Al_5Cu_2Mg_8Si_6$ and θ-Al_2Cu, while β-Mg_2Si phase is not preferred. To form θ-Al_2Cu and Q-$Al_5Cu_2Mg_8Si_6$ simultaneously, the Cu/Mg ratio was maintained more than 0.65 in the present work.

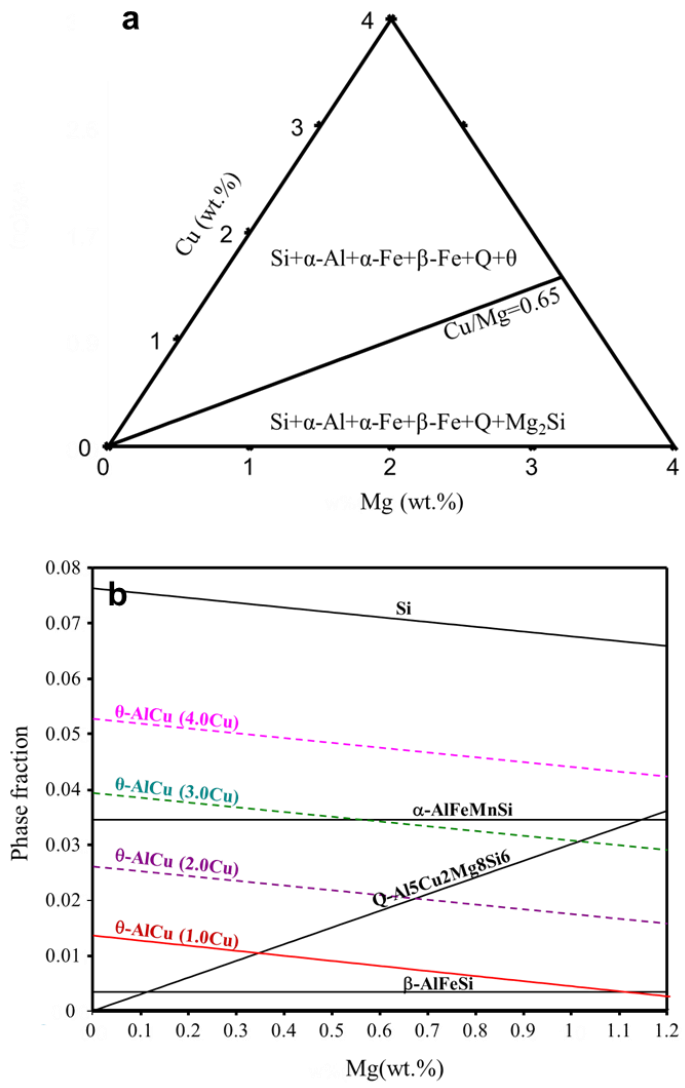

Figure 1. (a) Isothermal section and (b) phase fractions of Al-8.2Si-0.8Fe-0.5Mn-Cu-Mg alloys at 100℃ calculated by Pandat software.

It has been well-known that the strengthening of secondary phases in Al alloys is determined by several factors: (1) phase types, (2) volume fraction of the phase, (3) size, morphology and distribution of the phase. Figure 1b shows the phase fractions of Q-$Al_5Cu_2Mg_8Si_6$ and θ-Al_2Cu as a function of Cu from 1.0% to 4.0% and Mg from 0.3% to 1.2% calculated by Padat software. It is found that the fraction of Q-$Al_5Cu_2Mg_8Si_6$ phase was increased linearly as Mg content but

had no obvious dependency on Cu content. Clearly, the fraction of θ-Al_2Cu phase was determined by both Mg and Cu levels. There existed a negative liner relationship with Mg levels but a positive liner relationship with Cu levels. The prerequisite of a high strength alloy is the formation of enough strengthening phases. However, except the fraction, the strengthening effect is also affected by the morphology, size and distribution. Although Q-$Al_5Cu_2Mg_8Si_6$ is the preferred strengthening phase according to above analysis, the exceeding Q-$Al_5Cu_2Mg_8Si_6$ phase will lead to the coarsening and even segregation in the microstructure, which would definitely worsen the strength-ductility trade-off. Therefore, other phases such as θ-Al_2Cu phase is also needed to introduce synergistic strengthening together with Q-$Al_5Cu_2Mg_8Si_6$ phase. It is supposed that a roughly equivalent fractions of Q-$Al_5Cu_2Mg_8Si_6$ and θ would be helpful to obtain a desired microstructure and thus an attractive strength-ductility balance. Unfortunately, the morphology, size and distribution of strengthening phases cannot be accurately predicted by CALPHAD and/or other modelling methods. Therefore, to obtain the optimum strength-ductility balance, a series of Al-Si alloys synergistically strengthened by both Q-$Al_5Cu_2Mg_8Si_6$ and θ-Al_2Cu phases were designed and tested. In the experimental study, Cu and Mg variations were set as 2%-4% and 0-1.2%, respectively. All the Cu/Mg ratios are more than 0.65 to ensure the formation of Q-$Al_5Cu_2Mg_8Si_6$ and θ-Al_2Cu phases.

In die-cast alloys, Fe is unavoidable and useful to prevent die soldering in association with the benefit of using recycled secondary materials to make alloys with lower cost. Generally, Mn is also added to eliminate the detrimental effect of Fe by supressing the formation of needle-like β-Fe phase [25-28]. Therefore, Fe and Mn are added in the designed alloys during experimental validation.

3. Experimental process

A series of experimental alloys were prepared by melting commercial pure Al, Cu and Mg ingots, Al-10Sr, Al-50Si and Al-20 Mn master alloys. Firstly, each raw material was weighted against the target composition. Then Cu, Si, Mn were loaded into a clay-graphite crucible using an electric resistance furnace at 780 ˚C to obtain a melt. Afterwards, Mg ingot and Al-10Sr master alloy, which were preheated to 200˚C, were added into the melt. After a half hour of homogenisation, degassing using commercial argon and fluxes was performed by a commercial rotatory degasser at 350 rpm for 5 min. After skimming, a mushroom casting for measuring composition was made, prepared and tested for the required composition, during which an adjustment may be needed to reach the target composition. After that, the melt at 690 °C was

manually dosed and subsequently released into the shot sleeve of a 4500 kN cold chamber HPDC machine equipped with a die for 8-off dog bone-shaped samples with a Φ6.35 mm and a gauge length of 50mm. The die was preheated by the circulation of mineral oil at 150°C in all shots. The composition of experimental alloys is summarised in Table 2.

Table 2. The composition of experimental alloys.

Element	Si	Cu	Mg	Fe	Mn	Sr
Wt.%	8.2±0.15	varied※a	varied※b	0.8±0.07	0.5±0.06	0.0015±0.0.0002

※a Cu contents were 2.0, 2.5, 3.0, 3.5 and 4.0, respectively, and the tolerance is 0.11.

※b Mg content were 0.3, 0.6, 0.9 and 1.2,respectively, and the tolerance is 0.06.

All samples were left at ambient temperature for 7 days before testing the tensile properties using an Instron 5500 Universal Electromechanical Testing Systems at ~ 25^{o}C at a rate of 1mm/min. For each alloy, at least 15 tensile samples were tested, and the average value was taken as the value of mechanical properties. For metallographic analysis, samples were cut from the middle of tensile sample, and then mechanically grounded and polished using a standard method. To observe the morphology of eutectic Si, Keller's reagent was used to deep-etch the matrix of samples for 10 to 20s. The microstructural characterization and phase identification were carried out using a scanning electron microscopy (SEM, Zeiss-Supra 35VP, Germany) equipped with an energy-dispersive x-ray spectroscopy (EDS) and a back-scattered diffraction (BSD).

4. Experimental results

4.1 Mechanical properties of Al-Si-Cu-Mg alloys

In experiments, 5 levels of Cu and 4 levels of Mg were adopted to validate the theoretical understanding. Therefore, 20 alloys with different Cu & Mg combinations were tested. For simplicity, contour maps (Figure 2) were applied to show the effect of Cu and Mg levels on the mechanical properties of experimental alloys. Figure 2 indicates that increasing the Cu or the Mg levels could improve the yield strength from 160 MPa to 230 MPa at the cost of elongation from 5.5% to 2.8%. Cu and Mg additions also improved the UTS from 330 MPa to 370 MPa, as shown in Figure 2c. However, as shown in the bottom right corner of Figure 2c, the high Cu & low Mg combination had a neglectable improvement in UTS. For example, the alloy with 4.0Cu0.3Mg had the UTS of 340 MPa, which was a little higher than the alloy with

2.0Cu0.3Mg for the UTS of 330 MPa. Figure 2d illustrates the composition range (marked by light green colour) providing the yield strength more than 200 MPa and the elongation more than 4.0%. It is found that the yield strength of 200 MPa can be achieved by several Cu & Mg combinations. While, these combinations could provide different elongations. As shown in Figure 2d the blue line represents the yield strength of 200 MPa, which could move to the area with higher Cu/Mg ratios or the area with higher Cu and lower Mg levels. The elongation was accordingly varied from 4.6% to 4.0%. It means that Mg could increase the yield strength at a lower cost of elongation in the experimental alloys. Considering that Mg was only able to form Q-$Al_5Cu_2Mg_8Si_6$ phase, it can conclude that Q-$Al_5Cu_2Mg_8Si_6$ phase provided more effective strengthening than θ-Al_2Cu phase did in the experimental alloys. However, the configuration of the lowest Cu/Mg ratio (i.e. highest Mg level and lowest Cu level) was also not good in industrial application because Mg was prone to be burned off and the increased Mg would cause difficulty in melting and composition control. Therefore, the balanced 3.0Cu and 0.9Mg were selected as the composition in the present work. The alloy with the composition of Al-8.2Si-3Cu-0.9Mg-0.8Fe-0.5Mn-0.015Sr is defined as BD5 alloy.

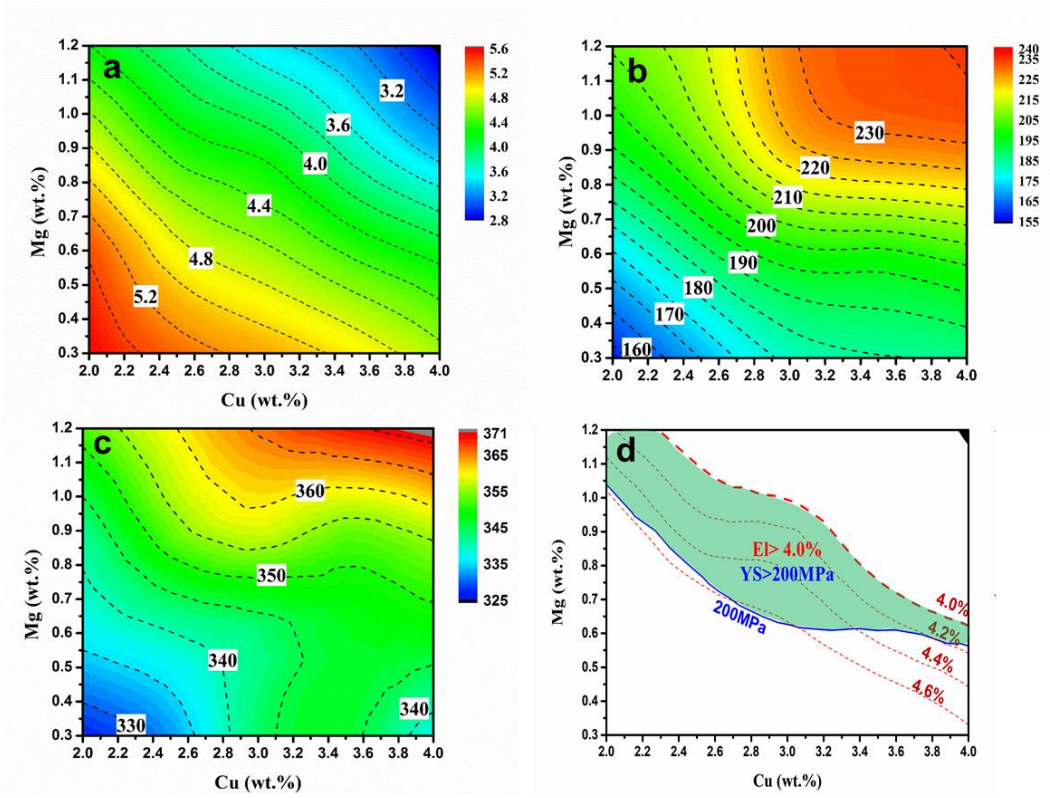

Figure 2. Effect of Cu and Mg levels on (a) elongation, (b) yield strength and (c) ultimate tensile strength of Al-8.2Si-Cu-Mg-0.8Fe-0.5Mn alloys, and (d) the composition range (green area) that provides the yield strength >200 MPa and the elongation >4.0%.

In order to understand the capability and repeatability of the experimental alloys, 36 tensile samples of the BD5 alloy were tested and shown in Figure 3a. The results confirmed that the yield strength was 225 MPa, the UTS was 361MPa and the elongation was 4.3%. For comparison, the properties of different alloys with high Mg level (3.0Cu1.2Mg), high Cu level (4.0Cu0.9Mg), and low alloying element (2.0Cu0.3Mg) were also plotted in Figure 3a. It shows that high Mg or Cu level only improved the strength slightly by 5-7 MPa but led to a significant loss in elongation, while too less 2Mg and Cu level (2.0Cu0.3Mg) could not provide a high strength. Therefore, the BD5 alloy obtained a satisfied balance of strength and elongation. Figure 3b shows the distribution of the yield strength and elongation of the BD5 alloy. It is seen that all measured values were within the larger squares defined by the two times of standard deviations, in which about 53% of the values (19 of 36) were within the smaller square representing the standard deviation. It means that the measured values contain no outlier and the variation is from random error. In other words, the properties of the BD5 alloy are robust and repeatable.

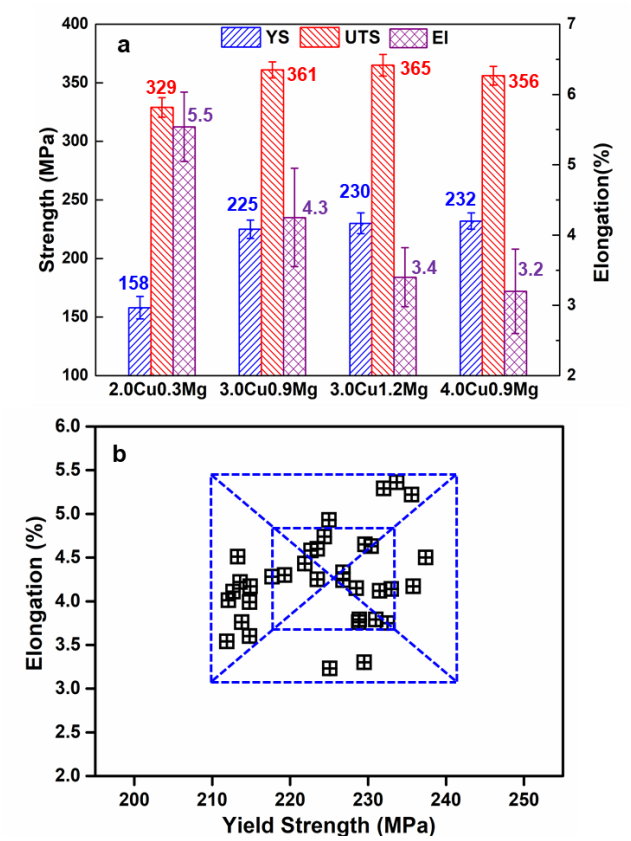

Figure 3. (a) Average tensile properties of experimental alloys, (b) the measured distribution of elongation and yield strength of the BD5 alloy. The squares represent the standard deviation and two times of standard deviations of the measured data.

4.2 Microstructure characterisation

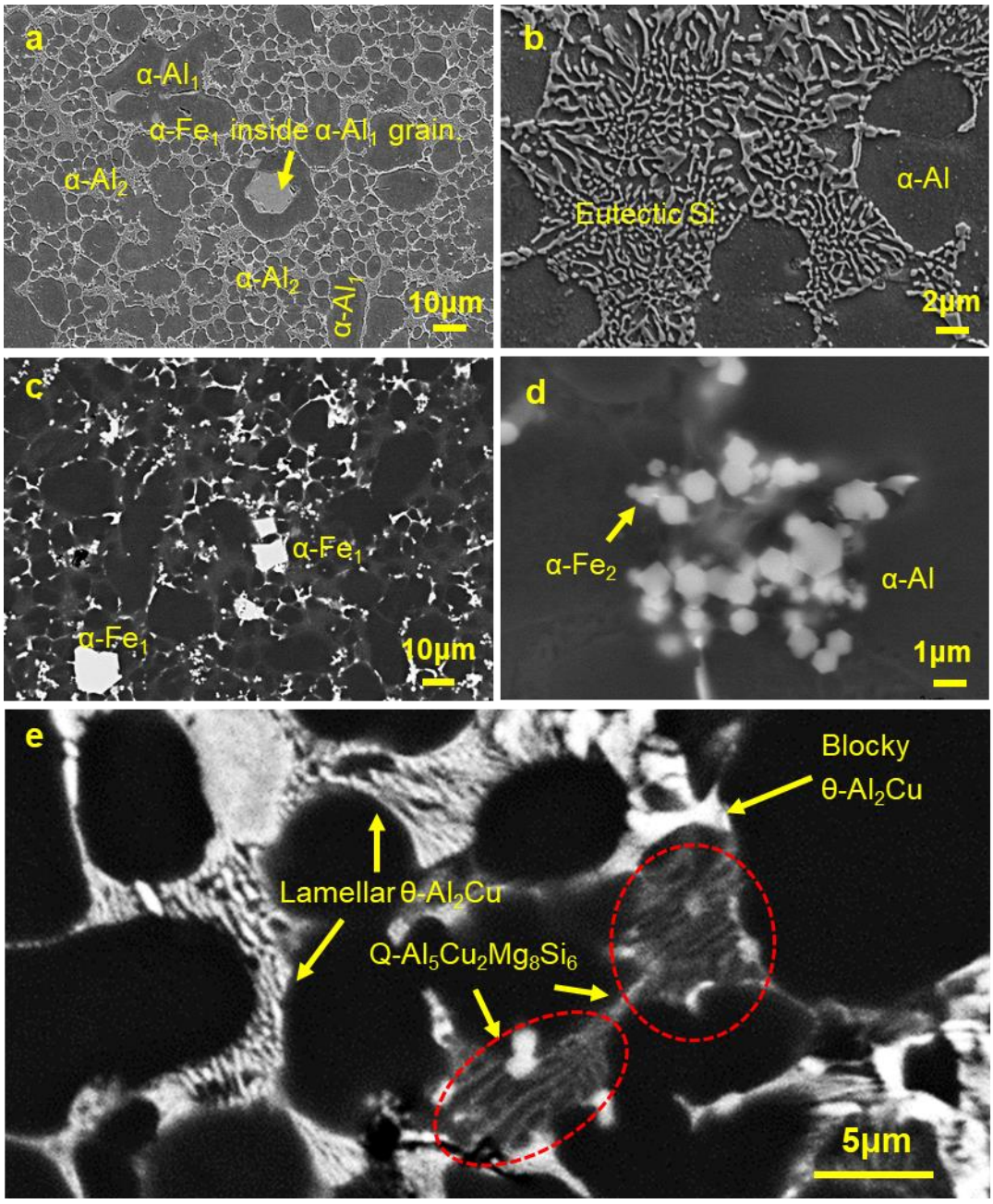

Figure 4. (a, b) SEM micrographs and (c-e) backscattered SEM micrographs of the BD5 alloy. (a, c) overall microstructure, (b) modified eutectic Si, (d) secondary α-Fe_2 particles, (e) θ-Al_2Cu phase and Q-$Al_5Cu_2Mg_8Si_6$ phase (marked by red circle).

The microstructure of the BD5 alloy is shown in Figure 4. It is found that the size of α-Al grains had a bimodal size distribution. The dominant fine globular grains (labelled as 'α-Al_2') were less than 10 μm, while a few coarse fragmented dendrites (labelled as 'α-Al_1') had a size range

from 20 to 80 μm. The formation of two sizes of the α-Al phase was due to the huge difference of cooling rate in the typical two-stage HPDC solidification process, during which the cooling rate was 10^2 K/s in the shot sleeve but reached up to 10^3 K/s in the die cavity [12, 29]. The results in Figure 4b revealed that the eutectic Si phase showed a coral-like morphology.

The different intermetallic were clearly illustrated by backscattered SEM micrographs in Figure 4c-e. Two types of compact α-$Al_{15}(Fe, Mn)_3Si_2$ phase with different sizes were observed in Figure 4c and d. The average size of the coarse Fe-rich intermetallic labelled as 'α-Fe_1' in Figure 4c was 16 μm, but that of fine Fe-rich intermetallic labelled as 'α-Fe_2' in Figure 4d was 0.75 μm. This phenomenon was also observed in our previous works and is attributed to the effect of different cooling rates in two-stage solidification in HPDC process [12]. An interesting phenomenon was also noticed for that some α-Fe_1 particles in the BD5 alloy was found in the centre of α-Al_1 grains (Figure 4a), although most of α-Fe_1 particles located in the boundary of α-Al grains. The needle-like β-Fe phase was not observed in the alloy although CALPHAD result (Figure 1b) predicted that the 0.3 mol.% β-Fe phase is possibly formed. The reason of difficulty in observation may attribute to the low level of β-Fe phase supposed to be formed from the non-equilibrium solidification of HPDC process. The white θ-Al_2Cu is another intermetallic phase distributed in the boundaries of α-Al grains. Two different morphologies of θ-Al_2Cu phase were observed as blocky and fine lamella in Figure 4e. The grey Q-$Al_5Cu_2Mg_8Si_6$ phase was also observed at α-Al grain boundaries with lamellar morphologies.

Table 3. The fraction (mol.%) of Q-$Al_5Cu_2Mg_8Si_6$ and θ-Al_2Cu phases in experimental alloys at 100°C calculated by Pandat software.

Alloy	2.0Cu0.3Mg	3.0Cu0.9Mg	3.0Cu1.2Mg	4.0Cu0.9Mg
Q	0.9	2.7	3.6	2.7
θ	2.3	3.2	2.9	4.5

Table 3 shows the fractions of Q-$Al_5Cu_2Mg_8Si_6$ and θ-Al_2Cu phases in the 4 experimental alloys calculated by Pandat software. The calculation results indicated that, in the alloy with 3.0Cu0.9Mg, the fraction of Q-$Al_5Cu_2Mg_8Si_6$ phase was 2.7 mol.% and that of θ-Al_2Cu phase was 3.2 mol.%, showing close fraction for these two phases in the same alloy.

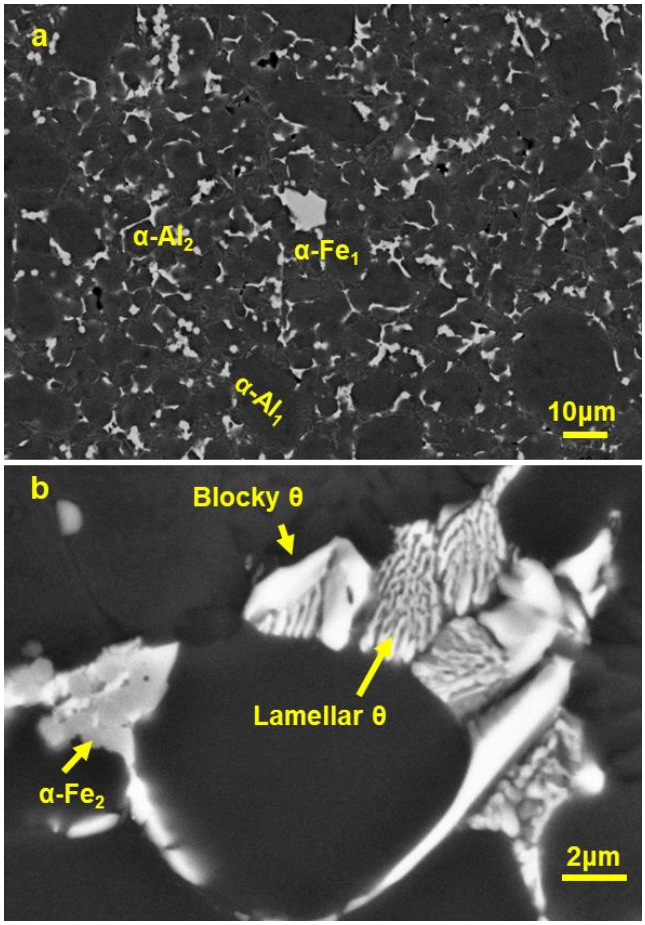

Figure 5. (a) overall and (b) magnified SEM micrographs showing the microstructure of the BD5 alloy.

After observing the overall microstructure, a confusing phenomenon was noticed. The amount of lamellar Q-$Al_5Cu_2Mg_8Si_6$ phase in the alloy with 3.0Cu0.9Mg is much less than that of θ-Al_2Cu phase. Meanwhile, it was also found that no Q-$Al_5Cu_2Mg_8Si_6$ phase was observed in the alloy with 0.3Mg (as shown in Figure 5), although the CALPHAD results in Table 3 predict that the alloy with 2.0Cu0.3Mg contains non-negligible 0.9 mol.% of Q-$Al_5Cu_2Mg_8Si_6$ phase. This result is in good agreement with our previous work [11], in which Q-$Al_5Cu_2Mg_8Si_6$ phase was also not observed in the Al-9Si-3.5Cu-Mg alloy until Mg level reached up to 0.48%. These indicate that Q-$Al_5Cu_2Mg_8Si_6$ phase is probably existing in another format except the eutectic lamella. The possible reasons for not able to observe these are: (1) Q-$Al_5Cu_2Mg_8Si_6$ phase may show in a similar colour or very small difference with α-Al matrix in backscattered SEM micrographs, (2) Q-$Al_5Cu_2Mg_8Si_6$ phase may be too fine to be seen in SEM. To observe the Q-$Al_5Cu_2Mg_8Si_6$ phase in other formats, two methods were simultaneously adopted : (1) In-lens micrographs, which are produced by pure secondary electrons (normal secondary electron

micrographs are produced by secondary electrons with a small backscattered electrons) and thus have higher spatial resolution and a clear edge effect; (2) A longer etching time (20s), which is helpful to expose the possible small Q-$Al_5Cu_2Mg_8Si_6$ phase and give a more obvious edge effect.

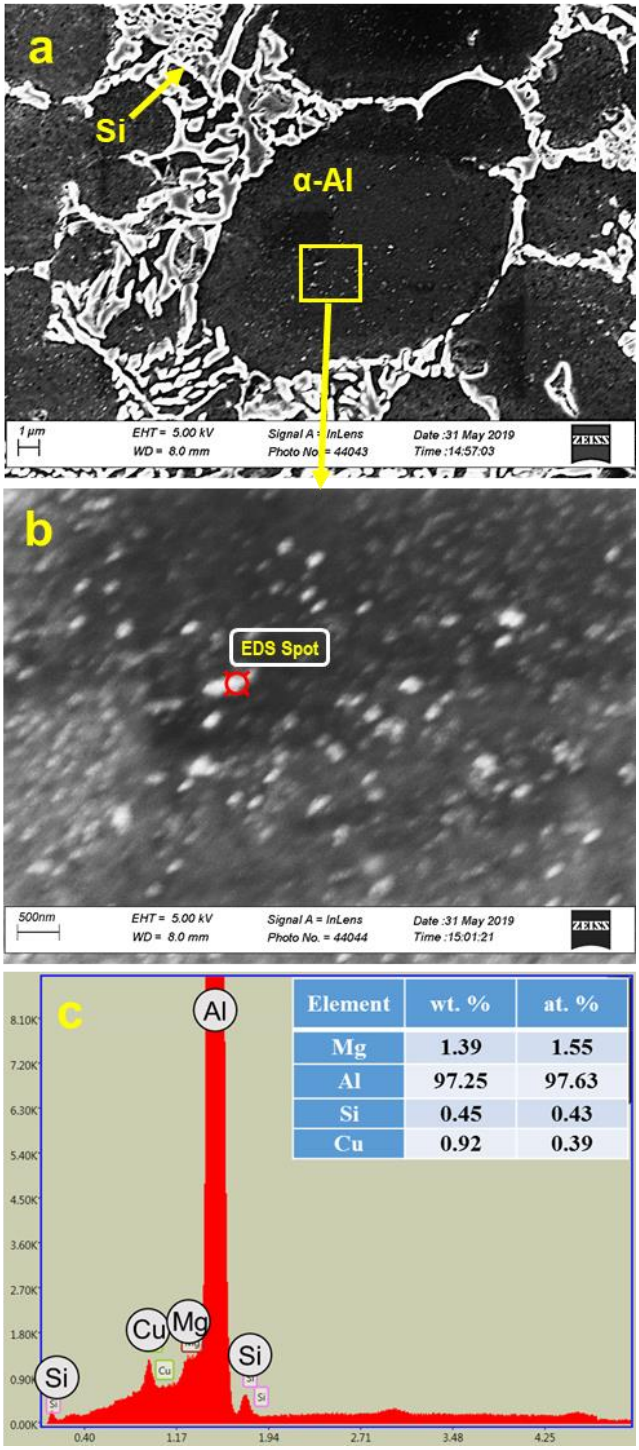

Figure 6. (a, b) In-lens micrographs and (c) EDS result of small precipitations inside α-Al grains in the BD5 alloy.

Figure 6 shows the in-lens SEM micrographs and the corresponding EDS results. Benefiting from the obvious edge effect, numerous fine white precipitates inside α-Al grains were observed. The in-lens SEM micrograph with a higher magnification provides more details in Figure 6b. It is found that numerous small precipitates were evenly distributed inside the α-Al grains and the majority of these particles were less than 200 nm, while a few large precipitates were up to 500 nm. Normally, nanoscale precipitates are formed through solutionising and ageing process during heat treatment. But in Figure 6, these were observed in the as-cast microstructure without solutionising and ageing treatment. The EDS analysis was performed on the precipitate and the typical result was shown in Figure 6c. It indicates that the precipitate is composed of Al, Si, Cu and Mg elements. According to the CALPHAD results in Figure 2, the Mg-rich and Cu-rich phases in the BD5 alloy are θ-Al_2Cu and Q-$Al_5Cu_2Mg_8Si_6$. However, θ-Al_2Cu phase with the size range up to 500nm would be detected as brilliant white particles in backscattered SEM micrographs (Figure 4 c-e), which is not in agreement with the observed result in Figure 6. Besides, the Mg/Cu atomic ratio of precipitates was detected as 1:4, which is the exact same with the Mg/Cu atomic ratio of Q-$Al_5Cu_2Mg_8Si_6$ phase. Therefore, the precipitates could be considered as Q-$Al_5Cu_2Mg_8Si_6$ phase. Recently, similar results have been reported by Zuo [20], who found that the small precipitates in the Al matrix of as-cast Al-Si alloys are Q-$Al_5Cu_2Mg_8Si_6$ phase and the size varied from 0.2 μm to 1.2 μm, which is much larger than the Q-$Al_5Cu_2Mg_8Si_6$ precipitates in Figure 6. It is also noticed that the Si content in the precipitates was lower than that in Q-$Al_5Cu_2Mg_8Si_6$. In fact, Q-$Al_5Cu_2Mg_8Si_6$ phase doesn't have a specific composition and the variations in the composition of Q-$Al_5Cu_2Mg_8Si_6$ phase have been reported by several researchers [21, 30, 31]. The detailed formation mechanism and composition of Q-$Al_5Cu_2Mg_8Si_6$ precipitates need more experimental evidences.

As shown in Figure 3a, the increased Mg (1.2%) or Cu addition (4.0%) would further increase the yield strength of 5-7 MPa but reduce the elongation of 1% of the as-cast alloys in comparison with the BD5 alloy. In other words, the strength-ductility trade-off is not cost-effective anymore. To understand the underlying reasons, the microstructure of the as-cast alloys with 3.0Cu1.2Mg and 4.0Cu0.9Mg were further studied and the results are shown in Figure 7. It is found that the vast majority of θ-Al_2Cu phase in the as-cast alloy with 3.0Cu0.9Mg showed granular morphology and the lamellar θ-Al_2Cu phase was hardly observed. It is also noticed that, compared with the as-cast alloy with 3.0Cu0.9Mg, the alloy with 3.0Cu1.2Mg had more Q-$Al_5Cu_2Mg_8Si_6$ lamellas but less θ-Al_2Cu phase. This microstructural change is agreed with the CALPHAD results shown in Table 3. However, the

fraction of white θ-Al_2Cu phase was 4.5 mol.% in the as-cast alloy with 3.0Cu1.2Mg, but that was 3.2 mol.% in the as-cast alloy with 3.0Cu0.9Mg, although the fraction of Q-$Al_5Cu_2Mg_8Si_6$ phase remained the similar of 2.7 mol.% in these two alloys. Moreover, θ-Al_2Cu phase tended to form clusters and became slightly coarse (Figure 7c).

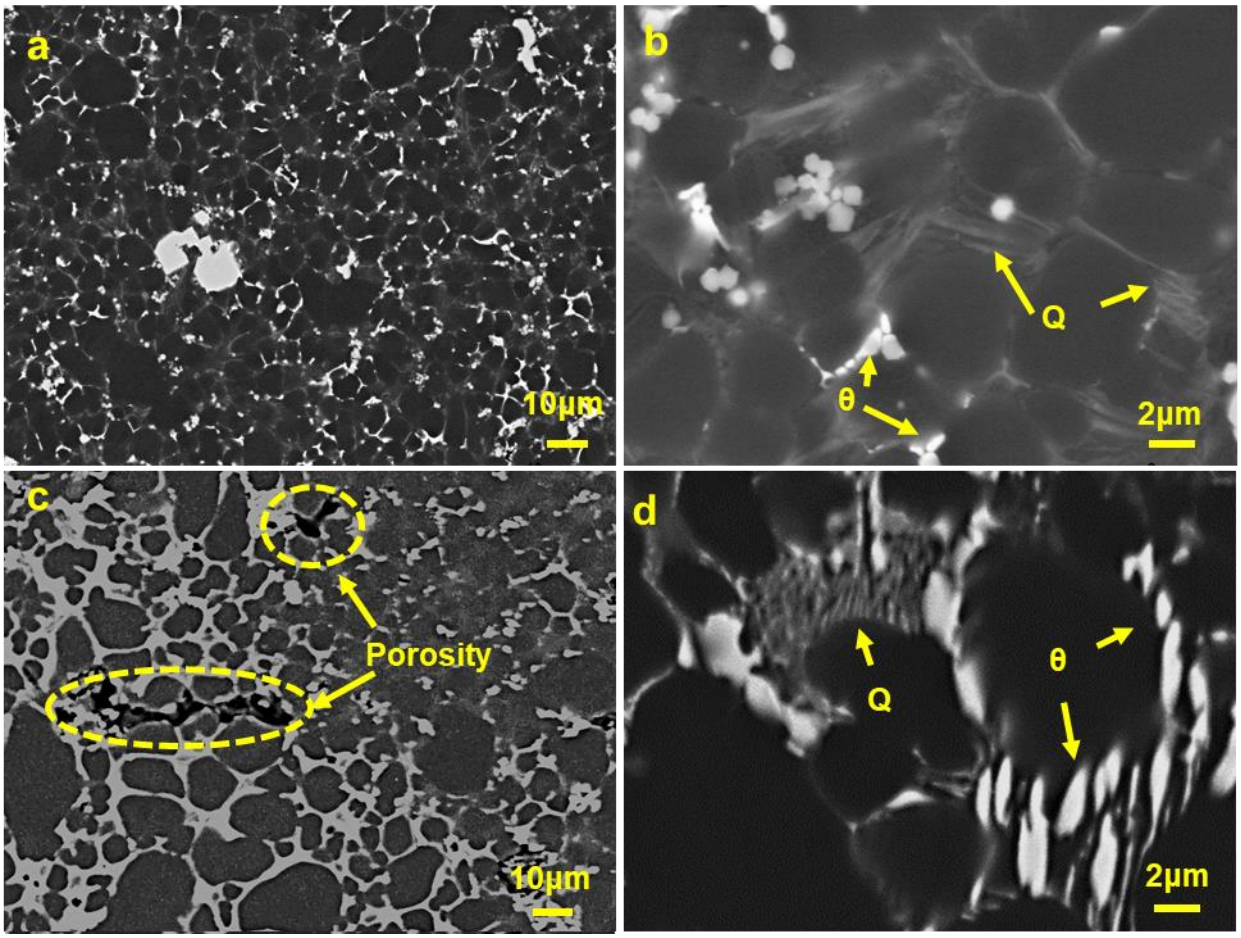

Figure 7. SEM micrographs showing the microstructure of the experimental alloys, (a, b) 3.0Cu1.2Mg and (c, d) 4.0Cu0.9Mg.

5. Discussion

5.1 Microstructure-solidification relationship

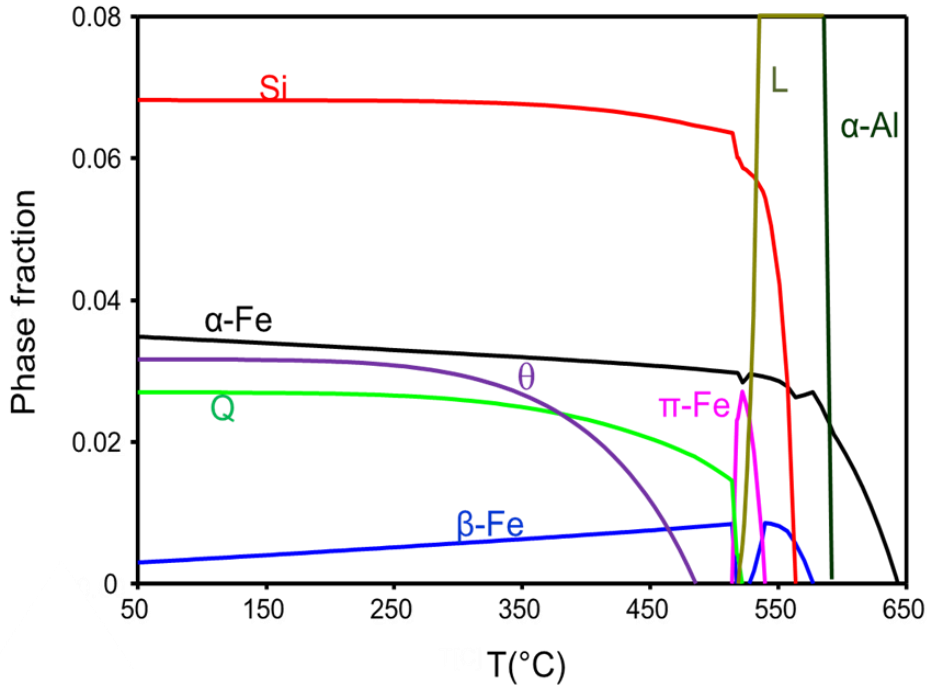

Figure 8. The phase fraction variation during the solidification of the BD5 alloy calculated by Pandat software.

By observing the microstructure in Figures 4-7, three interesting microstructural characteristics about α-Fe, Q-$Al_5Cu_2Mg_8Si_6$ phases and porosity were noticed: (1) some α-Fe_1 particles inside α-Al_1 grains were found in the experimental alloy with 3.0Cu0.9Mg (as shown in Figure 4a), but most of α-Fe particles distributed at α-Al grain boundaries; (2) as a strengthening phase, Q-$Al_5Cu_2Mg_8Si_6$ phase existed in two formats of large eutectic lamella at grain boundaries and nanoscale precipitates inside α-Al grains, of which the lamellar Q-$Al_5Cu_2Mg_8Si_6$ phase was observed only in the alloys with high Mg levels (0.6% and 0.9%); (3) in the alloy with 4.0Cu0.9Mg, several large porosities were appeared in the as-cast samples. To understand these phenomena, the solidification processes of alloys were calculated by Pandat software and the results are shown in Table 4.

Figure 8 and Table 4 showed that the primary α-Fe phase in the BD5 alloy precipitated directly from the melt by the reaction (L→α-Fe, 593°C-643°C) prior to the formation of primary α-Al grains. When the α-Al phase was formed at 593°C, the fraction of α-Fe phase reached to 2.1 mol.%. According to Yang's study [32], α-Fe has a semi-coherent interface (misfit of 2.67%)

with α-Al phase and thus is a potential nucleating substrate for α-Al phase. The existence of plenty α-Fe particles in the melt could provide the bases for nucleating α-Al phase, thus α-Fe_1 particles could be in the centre of α-Al_1 grains, as shown in Figure 4a. In the subsequent solidification at the temperature range of 536-593°C, α-Al and α-Fe phases continued to precipitate from the melt, but the nucleation of primary α-Al grains have finished so the newly formed α-Fe particles had no chance to be nucleating substrates for α-Al phase. As a result, the α-Fe particles would be pushed into the grain boundary area.

Table 4. The solidification steps in the BD5 alloy calculated by Pandat software.

Stage	Temperature range(℃)	Phase	Reaction
S1	>643	L	--
S2	593-643	α-Fe+L	L→α-Fe
S3	577-593	α-Al+α-Fe+L	L→α-Fe+α-Al
S4	563-577	β-Fe+α-Fe+α-Al+L	L+α-Fe→α-Al+β-Fe
S5	539-563	Si+β-Fe+α-Fe+α-Al+L	L→α-Fe+α-Al+β-Fe+Si
S6	525-539	π-Fe+Si+β-Fe+α-Fe+α-Al+L	L+β-Fe→α-Fe+α-Al+π-Fe+Si
S7	522-524	π-Fe+Si+α-Fe+α-Al+L	L+α-Fe→α-Al+Si+π-Fe
S8	519-522	Q+π-Fe+Si+α-Fe+α-Al+L	L+π-Fe→α-Fe+α-Al+Si+Q
S9	512-518	Q+π-Fe+Si+α-Fe+α-Al	α-Al+π-Fe→α-Fe+Si+Q
S10	485-511	Q+β-Fe+Si+α-Fe+α-Al	α-Al+β-Fe→α-Fe+Si+Q
S11	108-485	θ+Q+β-Fe+Si+α-Fe+α-Al	α-Al+β-Fe→α-Fe+Si+Q+θ
S12	<108	θ+Q+β-Fe+Si+α-Fe+α-Al	β-Fe→α-Fe+α-Al+Si+Q+θ

The second interesting phenomenon is that Q-$Al_5Cu_2Mg_8Si_6$ phase showed large eutectic lamellar at grain boundaries but nanoscale compact morphologies inside α-Al grains. What's more, the lamellar morphology was only observed in the alloys with high Mg levels (0.6% and 0.9%), and not found in the alloys with 0.3Mg. This phenomenon is also closely related with the solidification process. In the BD5 alloy, Q-$Al_5Cu_2Mg_8Si_6$ phase was precipitated from melt by the eutectic-like reaction (L+π-Fe→α-Fe+α-Al+Si+Q) at 519-522°C. After that, Q-$Al_5Cu_2Mg_8Si_6$ phase would precipitate through solid reaction, which usually occurred under 440°C, as shown in Figure 9a. Because of the easy diffusion and growth rate is relatively quicker in liquid state, eutectic lamella could be larger at the grain boundaries, as shown in Figures 4 and 7. On the other hand, for the nanoscale Q-$Al_5Cu_2Mg_8Si_6$ phase inside α-Al grains, the precipitation was in the solid state and the reaction is slow, resulting in the formation of compact particles to maintain their minimum surficial energy. Here another thing should be noticed. From the calculated results shown in Figures 8, 9 and Table 4, it is known that θ-Al_2Cu

phase was also precipitated only from supersaturated solid α-Al phase when Cu level was less than 4%. However, θ-Al_2Cu tended to locate in α-Al grain boundary area, rather than inside Al grains. This difference is the result of different mobility of their precursors (also called atomic clusters) in supersaturated solid α-Al phase. Grain boundary has a higher free energy than grain matrix, and thus tends to be the place where precipitates nucleated. If the precursor of phase moves very slowly, it needs a much longer time to reach grain boundary, during which the temperature of solidifying alloy decreases continually, resulting in a significant increase of undercooling for this specific phase. In this case, the increased number of the phase nucleation inside α-Al grains can be triggered by the large undercooling. Therefore, the precipitated phase will stay inside α-Al grains with very fine morphology. The distributions of Q-$Al_5Cu_2Mg_8Si_6$ and θ-Al_2Cu phases in the experimental alloys are related with the mobility of their precursors in Al grains. However, there has been no report for the study of the mobility of the precursors, the further study in future is needed to understand the detailed mechanism.

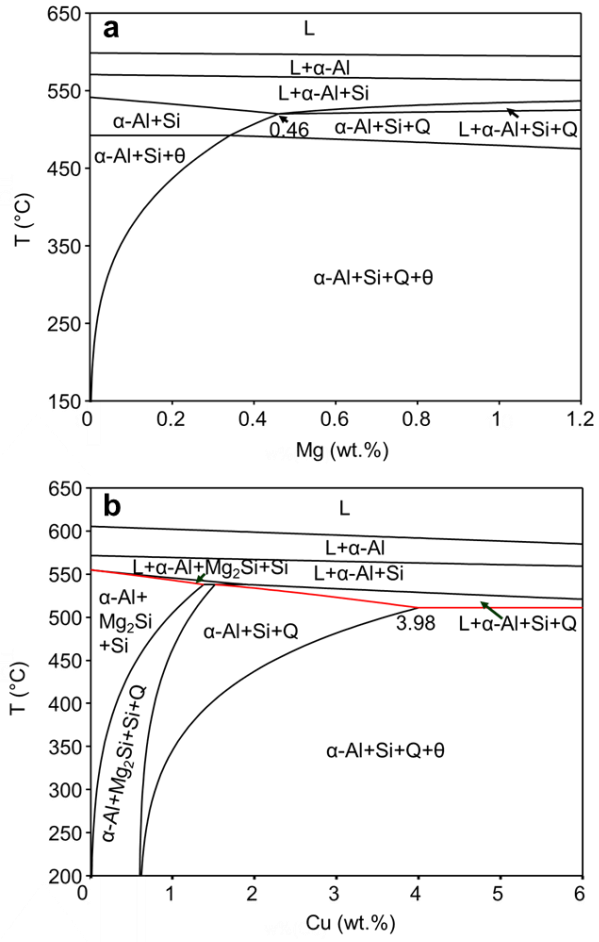

Figure 9. The cross section of equilibrium phase diagram of (a) Al-8.2Si-3Cu-xMg-0.8Fe-0.5Mn and (b) Al-8.2Si-xCu-0.9Mg-0.8Fe-0.5Mn alloys calculated by Pandat software.

The last phenomena studied in the present work is the formation of large porosities in the alloy with 4.0Cu0.9Mg (as shown in Figure 7c). From Figure 9b, it can be found that the increase of Cu levels in the alloy can decrease the solidus temperature (red line) until Cu level reaches 3.98%. In other words, the increment of Cu level leads to the increase of eutectic liquid pools at lower temperatures when the bulk alloy is already in solid state. Thus, the feeding into these liquid pools is more difficult, resulting in the formation of more porosities. Meanwhile, Cu accumulates to higher levels in the eutectic liquid pool, and the volumetric shrinkage during solidification increases [21, 33-35], which also promote the formation of porosities.

5.2 Microstructure-property relationship

The die-cast BD5 alloy based on Al-Si-Cu-Mg system can provide the yield strength of 225 MPa and the elongation of 4.3 % under as-cast condition (Figure 3). There is a significant improvement of more than 30% in the yield strength in comparison with the conventionally available die-cast alloys such as A380 used in industry, while the elongation is at the similar level. This is closely associated with the microstructural characteristics. The as-cast microstructure in the die-cast alloy consists of primary α-Al phase, Al-Si eutectics, α-Fe, Q-$Al_5Cu_2Mg_8Si_6$ and θ-Al_2Cu intermetallic phases. Among these, Q-$Al_5Cu_2Mg_8Si_6$ and θ-Al_2Cu phases strengthen the alloy by acting as pins to prevent dislocations from sliding under stress. However, the intermetallic themselves can initialise cracks, resulting in the reduction in elongation. Therefore, the main effort in the present work was to optimize the synergistic strengthening effect of Q-$Al_5Cu_2Mg_8Si_6$ and θ-Al_2Cu phases to balance the strength increase at a minimum scarification of elongation. Microstructural observation indicated that a large number of nanoscale Q-$Al_5Cu_2Mg_8Si_6$ precipitates are formed through the solid reaction inside the primary α-Al grains, and the lamellar Q-$Al_5Cu_2Mg_8Si_6$ phase can be precipitated directly from the melt to locate at the boundaries of α-Al grains. Benefitting from the fine size and relatively uniform distribution, nanoscale Q-$Al_5Cu_2Mg_8Si_6$ precipitates provide effective strengthening in the alloy. When Mg level is further increased from 0.9% to 1.2%, the exceeding lamella Q-$Al_5Cu_2Mg_8Si_6$ phase is formed in grain boundary area, which significantly weaken the elongation because of the easy formation of cracks under loads. When Cu level is increased from 3.0% to 4.0%, θ-Al_2Cu phase becomes coarse and segregates as clusters, which also weaken the strengthening effect in the alloy. What's more, the increased Cu promotes the formation of porosities, which are detrimental for the elongation of the alloy. Therefore, the optimised trade-off between strength and ductility can be achieved by the synergistic strengthening of Q-$Al_5Cu_2Mg_8Si_6$ and θ-Al_2Cu phases in the alloy.

5. Conclusions

(1) In as-cast Al-Si-Cu-Mg alloys, Q-$Al_5Cu_2Mg_8Si_6$ phase can be formed directly from the melt during solidification and from the solid state reaction in the solidified α-Al phase. The Q-$Al_5Cu_2Mg_8Si_6$ phase formed from liquid has a large lamellar morphology and aggregates at the boundaries of α-Al grains. The Q-$Al_5Cu_2Mg_8Si_6$ phase formed via solid state reaction has a fine compact morphology and distributes inside α-Al grains.

(2) In as-cast Al-Si-Cu-Mg alloys, the exceeding additions of Mg and/or Cu contents form too much strengthening phase and promote the formation of porosities in the as-cast alloy, resulting in an unacceptable reduction of elongation in the as-cast alloy.

(3) The Al-Si-Cu-Mg alloys for high pressure die casting can be optimised through the synergistic strengthening of Q-$Al_5Cu_2Mg_8Si_6$ and θ-Al_2Cu phases, which are closely related to the levels of Mg and Cu in the alloys.

(4) The alloy with the composition of Al-8.2Si-3Cu-0.9Mg-0.8Fe-0.5Mn-0.015Sr (defined as BD5 alloy) can offer the yield strength of 225MPa, the UTS of 361MPa and the elongation of 4.3% under as-cast condition. The significant improvement in the yield strength is more than 30%, while the elongation is maintained at the similar level, in comparison with the conventionally available die-cast alloys such as A380 used in industry.

Acknowledgements

Financial supports from Innovate UK (grant number 11019) and Jaguar Range Rover (grant number R33232) are gratefully acknowledged.

References

[1] Cecchel S, Panvini A, Cornacchia G. Low Solution Temperature Heat Treatment of AlSi9 Cu3(Fe) High-pressure die-casting actual automotive components. Journal of Materials Engineering and Performance 2018;27:3791-802.

[2] Dong X, Zhu X, Ji S. Effect of super vacuum assisted high pressure die casting on the repeatability of mechanical properties of Al-Si-Mg-Mn die-cast alloys. Journal of Materials Processing Technology 2019;266:105-13.

[3] Dong X, Yang H, Zhu X, Ji S. High strength and ductility aluminium alloy processed by high pressure die casting. Journal of Alloys and Compounds 2019;773:86-96.
[4] Zhu X, Blake P, Dou K, Ji S. Strengthening die-cast Al-Mg and Al-Mg-Mn alloys with Fe as a beneficial element. Materials Science and Engineering: A 2018;732:240-50.
[5] Ji S, Yan F, Fan Z. Development of a high strength Al-Mg_2Si-Mg-Zn based alloy for high pressure die casting. Materials Science and Engineering: A 2015;626:165-74.
[6] Ji S, Watson D, Fan Z, White M. Development of a super ductile diecast Al-Mg-Si alloy. Materials Science and Engineering: A 2012;556:824-33.
[7] Online Materials Information Resource - MatWeb. http://www.matweb.com/.
[8] Find Materials & Suppliers - Matmatch. https://matmatch.com/.
[9] Zolotorevsky VS, Belov NA, Glazoff MV. Casting Aluminum Alloys. 2007.
[10] Zhu X, Yang H, Dong X, Ji S. The effects of varying Mg and Si levels on the microstructural inhomogeneity and eutectic Mg2Si morphology in die-cast Al-Mg-Si alloys. Journal of Materials Science 2019;54:5773-87.
[11] Yang H, Ji S, Yang W, Wang Y, Fan Z. Effect of Mg level on the microstructure and mechanical properties of die-cast Al-Si-Cu alloys. Materials Science and Engineering: A 2015;642:340-50.
[12] Ji S, Yang W, Gao F, Watson D, Fan Z. Effect of iron on the microstructure and mechanical property of Al-Mg-Si-Mn and Al-Mg-Si diecast alloys. Materials Science and Engineering: A 2013;564:130-9.
[13] Ji S, Amirkhanlu F, Mostaed A, Beanland R. Atomic structure and interface chemistry in a high-stiffness and high-strength Al-Si-Mg/TiB_2 nanocomposite. Materials Science and Engineering: A 2019;763:138072.
[14] Du X, Gao T, Liu G, Liu X. In situ synthesizing SiC particles and its strengthening effect on an Al-Si-Cu-Ni-Mg piston alloy. Journal of Alloys and Compounds 2017;695:1-8.
[15] Hu Q, Zhao H, Li F. Microstructures and properties of SiC particles reinforced aluminum-matrix composites fabricated by vacuum-assisted high pressure die casting. Materials Science and Engineering: A 2017;680:270-7.
[16] Jung JG, Ahn TY, Cho YH, Kim SH, Lee JM. Synergistic effect of ultrasonic melt treatment and fast cooling on the refinement of primary Si in a hypereutectic Al-Si alloy. Acta Materialia 2018;144:31-40.
[17] Samuel A, Garza-Elizondo G, Doty H, Samuel F. Role of modification and melt thermal treatment processes on the microstructure and tensile properties of Al-Si alloys. Materials & Design 2015;80:99-108.

[18] Eskin DG. Ultrasonic processing of molten and solidifying aluminium alloys: overview and outlook. Materials Science and Technology 2017;33:636-45.
[19] Mohamed A, Samuel F. A review on the heat treatment of Al-Si-Cu/Mg casting alloys. Heat Treatment-Conventional and Novel Applications 2012:55-72.
[20] Zuo L, Ye B, Feng J, Kong X, Jiang H, Ding W. Effect of Q-$Al_5Cu_2Mg_8Si_6$ phase on mechanical properties of Al-Si-Cu-Mg alloy at elevated temperature. Materials Science and Engineering: A 2017;693:26-32.
[21] Biswas A, Siegel DJ, Seidman DN. Compositional evolution of Q-phase precipitates in an aluminum alloy. Acta Materialia 2014;75:322-36.
[22] Wang F, Zeng Y, Xiong B, Zhang Y, Li X, Li Z, et al. Effect of Si addition on the microstructure and mechanical properties of Al-Cu-Mg alloy. Journal of Alloys and Compounds 2014;585:474-8.
[23] Li HY, Zeng CT, Han MS, Liu JJ, Lu XC. Time–temperature–property curves for quench sensitivity of 6063 aluminum alloy. Transactions of Nonferrous Metals Society of China 2013;23:38-45.
[24] Farkoosh AR, Pekguleryuz M. Enhanced mechanical properties of an Al-Si-Cu-Mg alloy at 300 °C: Effects of Mg and the Q-precipitate phase. Materials Science and Engineering: A 2015;621:277-86.
[25] Bidmeshki C, Abouei V, Saghafian H, Shabestari SG, Noghani MT. Effect of Mn addition on Fe-rich intermetallics morphology and dry sliding wear investigation of hypereutectic Al-17.5%Si alloys. Journal of Materials Research and Technology 2016;5:250-8.
[26] Bjurenstedt A, Casari D, Seifeddine S, Mathiesen RH, Dahle AK. In-situ study of morphology and growth of primary α-Al(FeMnCr)Si intermetallics in an Al-Si alloy. Acta Materialia 2017;130:1-9.
[27] Ferraro S, Fabrizi A, Timelli G. Evolution of sludge particles in secondary die-cast aluminum alloys as function of Fe, Mn and Cr contents. Materials Chemistry and Physics 2015;153:168-79.
[28] Dinnis CM, Taylor JA, Dahle AK. As-cast morphology of iron-intermetallics in Al-Si foundry alloys. Scripta Materialia 2005;53:955-8.
[29] Yu Wb, Liang S, Cao Yy, Li Xb, Guo Zp, Xiong Sm. Interfacial heat transfer behavior at metal/die in finger-plated casting during high pressure die casting process. China Foundry 2017;14:258-64.
[30] Wolverton C. Crystal structure and stability of complex precipitate phases in Al-Cu-Mg-(Si) and Al-Zn-Mg alloys. Acta Materialia 2001;49:3129-42.

[31] Matsuda K, Ikeno S, Uetani Y, Sato T. Metastable phases in an Al-Mg-Si alloy containing copper. Metallurgical and Materials Transactions A 2001;32:1293-9.
[32] Yang W, Ji S, Zhou X, Stone I, Scamans G, Thompson GE, et al. Heterogeneous nucleation of α-Al grain on primary α-AlFeMnSi intermetallic investigated using 3d sem ultramicrotomy and HRTEM. Metallurgical and Materials Transactions A: Physical Metallurgy and Materials Science 2014;45:3971-80.
[33] Shabestari SG, Moemeni H. Effect of copper and solidification conditions on the microstructure and mechanical properties of Al-Si-Mg alloys. Journal of Materials Processing Technology 2004;153-154:193-8.
[34] Cáceres CH, Djurdjevic MB, Stockwell TJ, Sokolowski JH. The effect of Cu content on the level of microporosity in Al-Si-Cu-Mg casting alloys. Scripta Materialia 1999;40:631-7.
[35] Dash M, Makhlouf M. Effect of key alloying elements on the feeding characteristics of aluminum-silicon casting alloys. Journal of Light Metals 2001;1:251-65.